Visual Neuroscience (2002), **19**, 781–792. Printed in the USA.
Copyright © 2002 Cambridge University Press 0952-5238/02 $16.00
DOI: 10.1017/S0952523802196088

Temperature effects on spectral properties of red and green rods in toad retina

PETRI ALA-LAURILA,[1] PIA SAARINEN,[2] RAULI ALBERT,[1] ARI KOSKELAINEN,[1] AND KRISTIAN DONNER[2]

[1]Laboratory of Biomedical Engineering, Helsinki University of Technology, FIN-02015 HUT, Finland
[2]Department of Biosciences, Division of Animal Physiology, FIN-00014 University of Helsinki, Finland

(RECEIVED July 31, 2002; ACCEPTED October 22, 2002)

Abstract

Temperature effects on spectral properties of the two types of rod photoreceptors in toad retina, "red" and "green" rods, were studied in the range 0–38°C. Absorbance spectra of the visual pigments were recorded by single-cell microspectrophotometry (MSP) and spectral sensitivities of red rods were measured by electroretinogram (ERG) recording across the isolated retina. The red-rod visual pigment is a usual rhodopsin (λ_{max} = 503.6 nm and 502.3 nm at room temperature (21°C) in, respectively, *Bufo marinus* and *Bufo bufo*), that of green rods (λ_{max} = 432.6 nm in *Bufo marinus*) belongs to the "blue" cone pigment family. In red rods, λ_{max} depended inversely and monotonically on temperature, shifting by −2.3 nm when temperature was raised from 0°C to 38°C. Green-rod λ_{max} showed no measurable dependence on temperature. In red rods, warming caused a relative increase of sensitivity in the long-wavelength range. This effect can be used for estimating the energy needed for photoexcitation, giving E_a = 44.3 ± 0.6 kcal/mol for *Bufo marinus* rhodopsin and 48.8 ± 0.5 kcal/mol for *Bufo bufo* rhodopsin. The values are significantly different ($P < 0.001$), although the two rhodopsins have very similar absorption spectra and thermal isomerization rates. Our recording techniques did not allow measurement of the corresponding effect at long wavelengths in green rods. Although spectral effects of temperature changes in the physiological range are small and of little significance for visual function, they reveal information about the energy states and different spectral tuning mechanisms of the visual pigments.

Keywords: Rhodopsin, Spectral sensitivity, Absorbance, Temperature effects, Activation energy

Introduction

The absorbance spectrum is the most important functional characteristic of a visual pigment, determining the energy band of electromagnetic radiation accessible for vision. While absorbance spectra are positioned at different locations on the energy (or wavelength) axis, as expressed by the wavelength of maximum absorbance (λ_{max}), they have been found to have the same basic shape across the entire range of λ_{max} values and species investigated (Dartnall, 1953; MacNichol, 1986). For a given chromophore (in vertebrates, retinal A1 or A2), a satisfactory description of all known spectra can be achieved with a template having λ_{max} as sole variable (Lamb, 1995; Govardovskii et al., 2000). However, this refers to data collected from different species with different "natural" body temperatures, and possible temperature effects on spectra have been disregarded. Yet it has long been known that there is a measurable effect even of minor changes in body temperature on the spectral sensitivity of vision in the long-wavelength end (de Vries, 1948), and in pigment extracts significant shifts in λ_{max} and spectral shape are observed when temperature is varied over wide ranges (St. George, 1952; Yoshizawa, 1972).

To assess the presence and significance of such effects in the living photoreceptor cell, we measured spectral changes of pigments *in situ* in toad rods under temperature changes broadly within the natural range of variation in body temperature. Our main object of study is the *Bufo marinus* red rod, a well-characterized "model" photoreceptor, where the thermal activation rate as well as the amino acid sequence of the rhodopsin are known (Baylor et al., 1980; Fyhrquist et al., 1998*a*). In addition, Lamb (1984) has investigated the temperature effects on *Bufo marinus* photocurrent and spectral sensitivity at 700 nm relative to 500 nm. One specific purpose of our work was to assess the accuracy of a method for determination of the energy needed for photoactivation from temperature effects on the long-wavelength slope (Srebro, 1966; Koskelainen et al., 2000). In this respect, we compare the rhodopsins of *Bufo marinus* and the closely related *Bufo bufo*. We also compare the temperature effects in *Bufo marinus* red rods with those measured in the short-wavelength-sensitive "green" rods (Krause, 1892; Liebman & Entine, 1968) of the same species. The

Address correspondence and reprint requests to: Petri Ala-Laurila, Laboratory of Biomedical Engineering, P.O. Box 2200, Helsinki University of Technology, FIN-02015 HUT, Finland. E-mail: Petri.Ala-Laurila@hut.fi

green-rod visual pigment has been sequenced in another anuran amphibian, the bullfrog, *Rana catesbeiana*, and its amino acid sequence shows more than 65% identity with blue-cone pigments of goldfish and chicken (Hisatomi et al., 1999), representing the M1 cone family of vertebrate pigments (Okano et al., 1992). In a urodelan amphibian, the tiger salamander, *Ambystoma tigrinum*, the pigment of the green rod has been shown to be identical to that of the blue-sensitive cone (Ma et al., 2001).

The peak of the rhodopsin absorption spectrum was found to shift systematically towards shorter wavelengths with rising temperature, and in the temperature interval studied here the change parallels interpolations from earlier studies of bovine and bullfrog rhodopsin extracts conducted over a three times wider temperature range (St. George, 1952). By contrast, the peak of the green-rod pigment did not shift perceptibly, indicating that the spectral tuning mechanism is different in this pigment where λ_{max} is slightly *blue*-shifted from that of the protonated chromophore Schiff base in solution (Vought et al., 1999). An increase in relative sensitivity at very long wavelengths with warming, as previously measured in several rhodopsins as well as frog L cone pigment (Srebro, 1966; Koskelainen et al., 2000), could here be demonstrated only for red rods. For green rods no such effect was apparent in the range where absorbance was sufficient to be reliably measured by our MSP (below *ca.* 530 nm). The effect on red rods can be used for estimation of the energy needed for photoactivation (E_a) indicating $E_a = 44.3 \pm 0.6$ kcal/mol for *Bufo marinus* and 48.8 ± 0.5 kcal/mol for *Bufo bufo* rhodopsin. Some uncertainty in this calculation results from the shift in λ_{max} and change in spectral shape around peak, which are not recognized by the simple models on which the estimation is based (Stiles, 1948; Lewis, 1955; Srebro, 1966). We show, however, that these limitations are of only minor importance. Thus there is a robust difference between the two toad rhodopsins, which are very similar with respect to λ_{max} and rates of thermal isomerization (Fyhrquist et al., 1998*b*; Firsov et al., 2002). This supports our earlier conclusion that there is no simple, universally valid relation between the latter properties and the photoactivation energy (E_a) estimated from the temperature effect on spectral sensitivity (Koskelainen et al., 2000).

Materials and methods

Animals, preparations, and solutions

The experiments were done on isolated retinas of adult cane toads, *Bufo marinus*, obtained from the Carolina Biological Supply Company (Burlington, NC) and adult common toads, *Bufo bufo*, caught in the wild in southern Finland. The toads were kept at room temperature and fed with mealworms and food pellets. Before an experiment a toad was dark adapted for *ca.* 15 h. It was decapitated, pithed on both sides of the cut, and both eyes were removed and cut open along the equator under weak red light ($\lambda > 680$ nm). The retina was isolated from the hemisected eye and detached from the pigment epithelium in cooled (*ca.* 15°C) Ringer solution of the following composition (mM): Na^+, 113; K^+, 2.5; Ca^{2+}, 1.0; Mg^{2+}, 1.5; Cl^-, 103; EDTA, 0.010 (only in ERG Ringer); and glucose, 10. The solution was buffered to pH 7.5 (at room temperature) with 6.0 mM HEPES and 6.0 mM HCO_3^-. In some recordings HCO_3^- was replaced by 12 mM HEPES. In that case the Cl^- concentration was 112 mM, but the other components remained the same. HEPES Ringer was bubbled with 100% O_2 and HCO_3^- containing Ringer with 5% CO_2/95% O_2. The temperature dependence of pK_a of HEPES buffer is $\Delta pK_a/°C \approx -0.0125$ (Good et al., 1966; Vega & Bates, 1976), and for bicarbonate buffer saturated with CO_2, $\Delta pK_a/°C \approx -0.007$ (Harned & Bonner, 1945; cf. also Lamb, 1984). Hence, the pH of the Ringer solution would be expected to decrease from 7.7 to 7.3 when temperature is changed from 0°C to 40°C. Control ERG experiments were performed to test possible pH effects on spectral sensitivity at constant temperature in the above-mentioned pH range (no effects were seen).

For the ERG recording, the isolated retina was placed photoreceptors upward in a specimen holder (Donner et al. 1988) and the upper (receptor) side was superfused by a constant flow (*ca.* 1.4 ml/min) of Ringer. The Ringer was modified as follows for all or some of the ERG experiments: (1) Sodium-L-aspartate (2 mM) was always added to block synaptic transmission to second-order neurons. (2) Leibovitz cell culture medium, L-15 (Sigma-Aldrich, Helsinki, Finland) (715 mg/l) was used in some experiments to improve the viability of the isolated retina. (3) In some experiments, Ba^{2+} (10 mM) was used during dissection and also added (50 mM) to the Ringer solution filling the lower electrode space of the specimen holder, that is, at the vitreal side. Barium ions suppress glial currents (Bolnick et al., 1979; Donner & Hemilä, 1985) by blocking certain potassium channels that occur at highest density at the end feet of Müller cells, near the vitreal surface of the retina (Newman, 1989). Control experiments where perfusion was switched from Ba^{2+}-free to Ba^{2+}-containing Ringer indicated no measurable effect on spectral sensitivity.

For the MSP recording, small pieces of retina were excised, placed in a drop of Ringer solution on a coverslip, and teased apart by thin needles. A small amount (10–15%) of dextran (Mol. wt. = 70 kDa) was added to the Ringer to prevent excess cell movements. The sample was covered with another coverslip and sealed with vaseline along the edges.

Temperature control

The temperature of the sample could be adjusted and measured with 0.1°C accuracy in both the MSP and the ERG recordings. The temperature was controlled by a small heat exchanger built into the specimen holder: a mixture of water and glycerol (1:1) was circulated through a brass plate on which the specimen chamber rested. The temperature of the heat exchange solution could be adjusted over the range −20–+100°C with a temperature bath (Grant LTD 6 G). In ERG recordings, the superfusate circulated through the heat exchanger before entering the retina. The temperature was monitored with a thermistor in the bath close to the retina. In MSP recordings, a thin (diameter *ca.* 0.2 mm) temperature probe, (IT-23, WPI, Sarasota, FL) was inserted into the sample chamber before the glass slips were sealed together with vaseline. The sample chamber was attached to the specimen holder with thermoconductive silicon grease at the edges. The specimen holder was shielded by insulating material to ensure constant temperature also in the small air space near the sample. In ERG recordings at low temperature, desiccating silica gel and a cold spot condenser cooled by liquid nitrogen were placed near the specimen holder in the light-tight Faraday cage in order to avoid noise problems due to condensation water.

Microspectophotometry (MSP) recordings

The MSP recordings were performed as reported by Govardovskii et al. (2000) with an instrument modified as described by Govardovskii and Zueva (2000). The mechanism of spectral scanning was

built from the head control mechanism of a Seagate ST-225 computer hard disk drive. In this design, the diffraction grating was attached to the head-moving lever moved by a stepper motor. It allowed fairly reproducible scanning in ~1-nm steps at a rate of up to 1300 nm/s (Govardovskii & Zueva, 2000). In our experiments a scanning speed of 250 nm/s was used. Light-intensity data were acquired at a rate of four readings per step, which were subsequently averaged. The wavelength λ was nonlinearly related to the step number, n:

$$\lambda = 2\,\frac{\sin(a + b\cdot n)}{d}, \tag{1}$$

where d is the grating's period, and a, b are constants determined during calibration. Thus the raw absorbance data were obtained at nonuniformly spaced points, mostly at fractional wavelengths. The recording program recalculated the result to whole wavelengths using linear interpolation between adjacent points. The position of the diffraction grating (and, hence, wavelength) was controlled *via* an optical marker attached to the motor shaft. The reproducibility of the wavelength calibration depends on the reproducibility of the position of the stepper motor, corresponding to a final error in wavelength below 0.2 nm in any single absorbance recording. The wavelength calibration was performed using a mercury lamp and neodymium glass that was previously characterized by a standard Hitachi 150-20 spectrophotometer. The same neodymium glass was recorded repeatedly during experiments to ensure that the calibration remained stable. The wavelength range scanned was 350–750 nm.

Cells from the same sample were recorded at four different temperatures (*ca.* 0, 8.5, 28.5, & 38°C). The accepted temperature variation while recording a cell sample from which the spectra were subsequently averaged was ± 0.5°C. The results on red rods in *Bufo marinus* are based on samples from five retinas (all from different animals), where in each case 40 single cells were recorded at 8.5°C and 40 cells at 28°C. This strictly "physiological" temperature range was extended by further recordings at 0 and 38°C (at both these temperatures, 20 cells from each one of five animals, i.e. 100 cells, were recorded). The results on green rods are pooled from recordings on (different) cell samples at 0°C (30 cells) and 38°C (42 cells), in both cases obtained from three animals.

In addition to the main body of recordings, one control experiment was performed on the same ten individual red rod cells first at 28.5°C, then at 8.5°C, and finally again at 28.5°C to assess whether spectral changes unrelated to temperature as such might occur during the course of an experiment. The temperature effects of this experiment were fully reversible and similar to those in the main body of recordings.

Electroretinogram (ERG) recordings

Relative spectral sensitivities of rods were determined from aspartate-isolated mass photoresponses recorded across the isolated retina (Donner et al., 1988; Koskelainen et al., 1994, 2000). In each experiment two spectra were recorded from the same retina, at 8.5 ± 0.5°C and 28.5 ± 0.5°C, respectively. These temperatures, while spanning a reasonably wide range, still remain well within the limits that may be naturally experienced by an active frog during 24 h. After dissection and after each temperature change the retina was allowed to adapt for 1–2 h. The order of temperatures was changed between experiments, although no effect of the order was observed.

Stimulation and recording

The retina was illuminated from the upper (receptor) side. Spectral sensitivity was measured using a set of narrow-band interference filters (Schott DIL or Melles Griot; transmission bandwidth *ca.* 10 nm). The transmission peaks covered the wavelength range 434–777 nm. A halogen lamp (50 W) driven by a stabilized current source provided the light for stimulation. Homogeneous full-field flashes (usually 20 ms) were used. The intensity was controlled with neutral density filters (Balzers) and a neutral wedge (Melles Griot). Light intensities were calibrated for each interference filter by means of a calibrated photodiode (EG&G HUV-1000B, calibrated at the National Standards Laboratory of Finland). The mass receptor potential was recorded with two Ag/AgCl sinter electrodes (WPI), one placed in the Ringer space under the retina and the other in chloride solution connected to the perfusion Ringer through a porous plug at the upper (receptor) side of the retina. The DC-signal was amplified 1000×, filtered by an active 8-pole Bessel-type low-pass filter with cut-off frequency 20 Hz, amplified again (10–100 ×), digitized at 200 Hz, and stored in the computer.

Isolation of responses from red rods

Even when synaptic transmission has been blocked by aspartate, the transretinally recorded signal may contain several components of different origins: rod responses from two types of rod, cone responses from at least two types of cone, and a glial (Müller cell) response to changes in the potassium concentration around the photoreceptors. Rod responses can be separated from cone responses on the basis of their kinetics (cf. Koskelainen et al., 2000). In the rod response, the green-rod component is negligible at wavelengths around and beyond red-rod λ_{max}. For example, at 502 nm the relative sensitivity of the red rods is more than ten times larger than that of the green rods and the difference increases with increasing wavelength. Moreover, red rods outnumber green rods in anuran retina by 7–10-fold (see e.g. Donner & Reuter, 1976), and their contribution to the mass response is correspondingly greater. The glial component in the rod response was not wholly eliminated even by the use of Ba^{2+}, but it affects the response mainly after peak. The absence of a significant glial contribution to the peak amplitude was checked by fitting the early part of the rod response with a model waveform derived from single-cell recordings (Baylor et al., 1974, 1979; cf. Fig. 1D, inset).

Recording protocol and analysis

The recording protocol and method for determining spectral sensitivity is illustrated in Fig. 1. Sensitivity at each test wavelength was determined in relation to a reference wavelength (519 nm) chosen reasonably close to the sensitivity peak (λ_{max}). Families of responses to 4–5 different flash intensities were recorded repeatedly at the reference wavelength. A generalized Michaelis function was fitted to each set of intensity–response (I–U) data thus obtained:

$$U = U_{max}\cdot\frac{I^n}{I^n + I_s^n}, \tag{2}$$

where U is the amplitude of the response, I is flash intensity, I_s is the half-saturating flash intensity, and n is a steepness parameter.

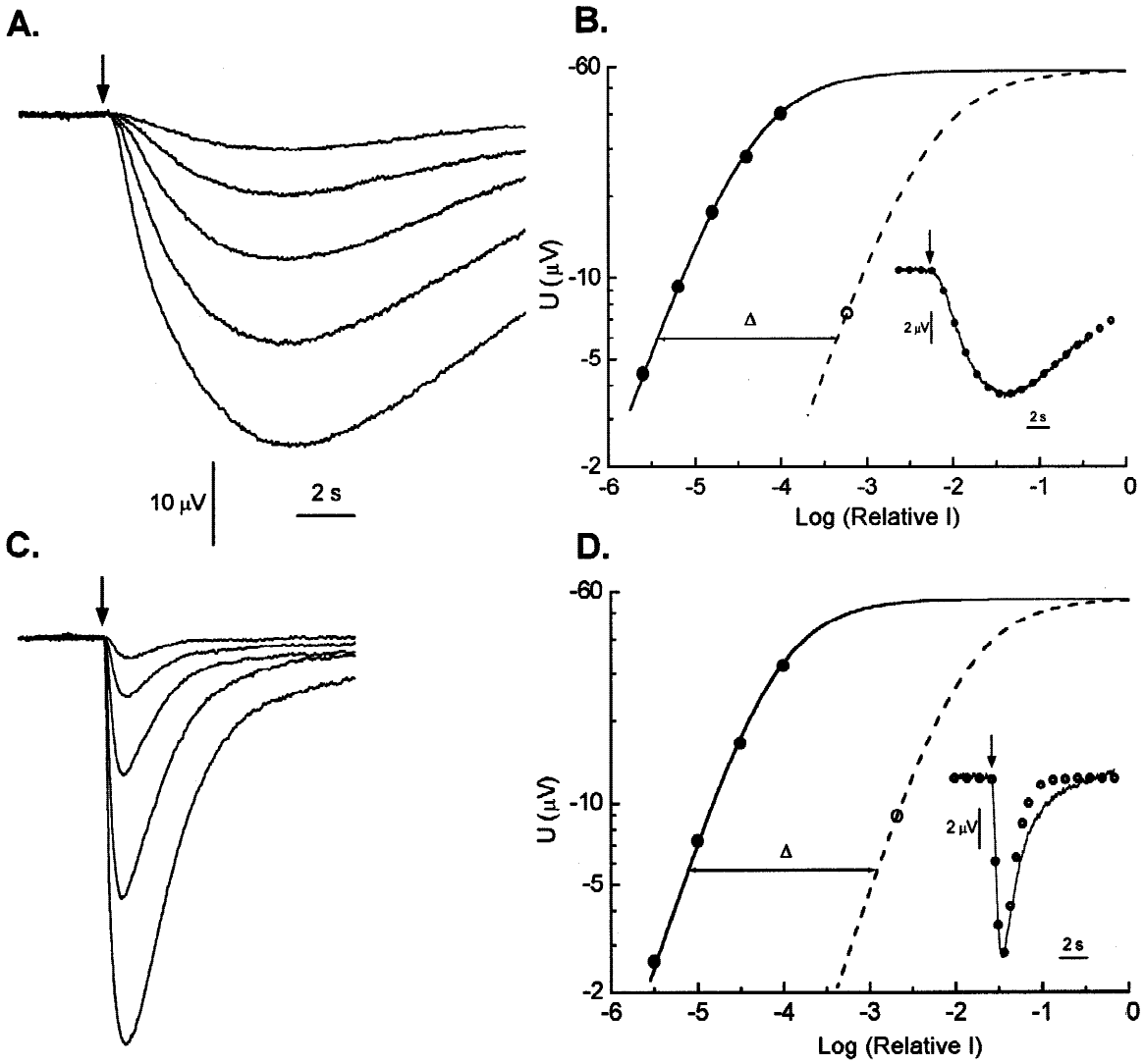

Fig. 1. Determination of spectral sensitivity of "red" rods by ERG recording from the isolated, aspartate-superfused retina of *Bufo marinus*. Panels (A) and (C) show families of responses to flashes of increasing intensity at the reference wavelength (519 nm) at 8.5°C and 28.5°C, respectively. The time of the stimulus flash (20 ms) is shown by an arrow. The largest responses are single recordings, the smaller ones are averages of 2–4. (B,D) Response amplitude *vs.* log flash intensity (the *I–U* function) at the reference wavelength (filled circles) was fitted with a modified Michaelis function [eqn. (2), continuous curve]. Series of 3–20 dim flashes at 3–5 different test wavelengths were recorded between two consecutive reference *I–U* functions. As an example, the averaged dim flash response at 638 nm is shown (inset), its amplitude is plotted on the log *I* scale (open circle), and the laterally shifted Michaelis curve that fits this test response (dashed line) is shown at both temperatures. Spectral sensitivity at each test wavelength was determined from the required lateral shift (Δ). The "test" responses shown are fitted with the "independent activation" model $U(t) = I\Delta tSn\alpha e^{-\alpha t}(1 - e^{-\alpha t})^{n-1}$ of Baylor et al. (1974) (small circles). The parameter values are $n = 3$ and $\alpha = 0.16$ for the response in (B) and $n = 3$ and $\alpha = 1.42$ in (D) .

Between the recordings of consecutive reference *I–U* functions, 3–20 dim-flash responses were recorded at each of 3–5 different test wavelengths. The intensity of "dim" test flashes was chosen to produce responses of amplitude less than 20% of the saturated response. Responses were averaged, baseline-corrected, and their amplitude was read. Spectral sensitivities were determined from the lateral shifts (Δ) on the log *I* axis required to make response amplitudes to the respective test wavelengths match the 519-nm Michaelis curve (see Fig. 1). Possible small changes in sensitivity from one reference *I–U* function to the next were corrected by linear interpolation between the corresponding Michaelis curves.

Determination of the energy for photoactivation of the visual pigment (E_a)

Constructing a composite spectrum from MSP and ERG data

Spectral properties of photoreceptor cells are best studied by MSP in the main absorbance range and by electrophysiology (here ERG) at very low absorbances. Electrophysiology then draws its advantage from the high physiological amplification of single isomerizations (especially so in dark-adapted rods) and, in ERG recording, also from the instantaneous averaging of responses from

thousands of rods. This permits measurements with high signal-to-noise ratio based on very sparse photon absorptions (on the order of one photon absorbed per 10^9 rhodopsin molecules). For normalized absorbances of a few percent and higher, on the other hand, MSP provides spectra of much higher quality than does electrophysiology with an equivalent investment of effort (cf. Govardovskii et al., 2000). Moreover, in the range around peak the rod ERG is connected with particular problems: (1) contamination by a green-rod component at shorter wavelengths; and (2) flattening of the spectrum due to rhodopsin "self-screening" under longitudinal incidence of the stimulating light (Dartnall & Goodeve, 1937; Alpern et al., 1987). Thus, we use MSP and ERG in the respective ranges where each is superior and "glue" the spectra together in a range 594–615 nm, where self-screening is negligible and both MSP and ERG give reliable readings. This gives us an accurate red-rod spectrum extending from 350 nm to 777 nm.

The joining together of the MSP and ERG spectrum was optimized as follows. A second-order polynomial was fitted to the averaged MSP data over the wavelength range 563–603 nm (we preferred to use an unbiased parabolic description rather than a regular visual-pigment template in this region, where the precise shape of the spectrum is temperature dependent). Above 600 nm the noisiness of the MSP data quickly increased, and the parabola extrapolated to 615 nm served to smooth the MSP spectrum in this range. The averaged ERG spectrum for the same temperature was then shifted vertically for best fit to the parabola according to a least-square criterion for three matching wavelengths (594, 601, & 615 nm). The ERG spectrum used was obtained by averaging individual spectra that were first vertically matched over the range 594–621 nm according to a least-square criterion.

The temperature effects were visualized also by means of warm–cold difference spectra (see Fig. 3C). The difference between "warm" and "cold" data at each wavelength was calculated separately for the MSP and the ERG, which yielded one MSP and one ERG difference spectrum. The vertical anchoring of the ERG to the MSP in this case was based on smoothing the MSP difference spectrum by extrapolating a straight line fitted over the range 503–553 nm (the region mainly affected by the λ_{max} shift) and then positioning the ERG by means of a least-square match of the points at 594, 601, and 615 nm to this line.

Determining E_a from composite "cold" and "warm" spectra

Stiles (1948) suggested that in the far "red" end of the spectrum the energy of photons is too low to excite the visual-pigment molecule, and photoactivation occurs only if the photon energy is supplemented by thermal energy. In other words, there is a wavelength λ_0 ($\geq \lambda_{max}$) where the photon energy (hc/λ_0) corresponds precisely to the lowest-energy electronic transition from the zero vibrational level of the ground state to the first excited state, and photons with energy $<hc/\lambda_0$ can activate only molecules that lie on higher vibrational energy levels. Since warming will increase the fraction of molecules occupying higher levels, the relative sensitivity to photons of lower energy (i.e. wavelengths $\lambda > \lambda_0$) will increase with warming. This effect allows estimation of the energy needed for photoactivation of the visual pigment, here termed the "activation energy," $E_a = hc/\lambda_0$.

Before describing the procedure, we would like to point out that Stiles' general (and highly plausible) idea potentially allows formulation of several similar models, differing in specific assumptions. Stiles (1948) assumed that the thermal distribution of molecules on higher vibrational levels follows the Boltzmann distribution. This original formulation yields several strong predictions, some of which are found to hold with high precision, whereas others hold only as qualitative approximations: (1) The final limb of spectra in the long-wavelength end when plotted as log sensitivity ($\log S$) against $1/\lambda$ should form a straight line. (2) The slope of this line should be $= hc/kT \ln 10$. (3) Accordingly, when spectra are measured at two different temperatures (cold, C, and warm, W), the ratio of slopes (warm/cold) in this domain should be $= T_C/T_W$ and the difference of slopes (warm − cold) should be $= hc(T_C - T_W)/kT_WT_C \ln 10$. In the present work, we find that prediction #3 concerning temperature effects (most relevant for us) is quite accurate. Therefore, we shall as a rule refer to the original Stiles (1948) formulation, unless otherwise stated. However, Stiles himself noted that the final slope of (human) spectra was too shallow, only *ca.* 79% of prediction #2. Moreover, contrary to prediction #1, $\log S$ *vs.* $1/\lambda$ does not form a perfectly straight line over the domain $\lambda > \lambda_0$: spectra are in fact slightly curved, with monotonically increasing slope. Lewis (1955) amended the theory by replacing the Boltzmann distribution (which is not appropriate for complex molecules with many vibrational modes, such as visual pigments) by a distribution derived by Hinshelwood (1940). With this modification, the shape of the long-wavelength limb of spectra as well as temperature effects can be accurately accounted for (the predictions about temperature effects remain essentially the same as in Stiles (1948), except in the vicinity of λ_0). The disadvantage of the new formula is that it contains an additional parameter besides E_a (the number of vibrational modes, m) and as we are not primarily interested in evaluating the details of particular models, we shall refer to Lewis (1955) mainly to demonstrate that, within this class of models, it is *possible* to find a physically plausible formulation that correctly predicts both absolute slopes and temperature effects. Using this more complex version for estimating E_a would not change the comparisons between pigments (see Discussion).

Our main method for calculating E_a and error limits from the temperature effect on long-wavelength sensitivity was the same as described by Koskelainen et al. (2000), with the difference that they used only ERG data whereas our present estimates are based on a combination of MSP and ERG. The method effectively uses every pair of data points (warm–cold) recorded in the temperature-sensitive long-wavelength domain to get as many independent estimates of E_a, rather than, for example, relying on a single crossing point of "warm" and "cold" spectra. It was originally used by Srebro (1966) to extract E_a from *Limulus* data and is based on Stiles' (1948) model, although like Lewis (1955) it allows that the long-wavelength limb may not be a perfect straight line.

The relative sensitivity values of the composite spectra (see above) are denoted $\log S_i$, with additional index W corresponding to "warm" spectra or C corresponding to "cold" spectra. The (ERG) difference $\log S_{Wi} - \log S_{Ci}$ at each "long" wavelength λ_i was converted into its photon energy equivalent through the equation:

$$\frac{hc}{\lambda_a} = E_a = \frac{hc}{\lambda_i} + \frac{hc}{T} \cdot \frac{[-\partial \log S/\partial(1/T)]_i}{[\partial \log S_C/\partial(1/\lambda)]_i}, \quad (3)$$

(Srebro, 1966). For the calculations,

$$[-\partial \log S/\partial(1/T)]_i = (\log S_{Wi} - \log S_{Ci})/(1/T_C - 1/T_W),$$

where $T = T_C$ and $[\partial \log S_C/\partial(1/\lambda)]_i$ is the local slope of the C-spectrum at λ_i, determined as the derivative of a second-order

polynomial fitted to the long-wavelength data. The statistical error of the estimate depends on two variance components: (1) Variance connected with the attachment of the ERG data to the MSP spectra, estimated by a "matching" mean square $s_\mu^2 = A_{\max}^2 \cdot SS_\mu/(m-1)$. Here, $A_{\max}$ is the largest value of the energy conversion factor $A_i = hc/[(1 - T_C/T_W)\partial \log S_C/\partial(1/\lambda)_i]$ in that data set (corresponding to the smallest local slope), SS_μ is the least-square sum obtained in the joining together of MSP and ERG spectra, and $m = 6$ is the number of data points used for this purpose. (2) Variance between the point estimates of E_a, estimated by a conventional "sample" mean square $s_\rho^2 = SS_\rho/(M-1)$. SS_ρ is the sum of squares of the sample and M is sample size, that is, the number of longer-wavelength data point pairs used for estimation ($M = 5$ for *Bufo marinus*, $M = 7$ for *Bufo bufo*). Since the anchoring of spectra and E_a estimation were based on nonoverlapping data sets, the estimator of total variance (denoted s_E^2) is a sum of s_μ^2 and s_ρ^2, where each is weighted by its respective degrees of freedom (df $= m - 1$ and $M - 1$, respectively). The total SEM of E_a is then $= s_E/\sqrt{M}$. Confidence limits and statistical testing were based on Student's *t*-test with the degrees of freedom of the appropriate variance measure in each case.

Results

Rhodopsin in "red" rods

Comparison of spectra at two temperatures

MSP and ERG recording were used in the respective ranges where each is superior and the spectra were "glued" together in the intermediate range where both give reliable readings (see Methods for details). Fig. 2 shows such composite spectra from red rods of the cane toad, *Bufo marinus*, recorded at our two standard temperatures, 8.5°C ("cold") and 28.5°C ("warm"). Panel A uses linear coordinates to display accurately the range around λ_{max}; panel B uses logarithmic ordinates (together with $1/\lambda$ abscissa, see below) to expand differences in the long-wavelength end. MSP data are shown as lines: red full-drawn (warm) and blue dashed (cold) and ERG data as symbols: blue pluses (cold) and open red squares (warm).

The "warm" spectrum is rather well fit by the A1 template of Govardovskii et al. (2000) with $\lambda_{max} = 503.9$ nm (not shown). By comparison, the "cold" spectrum is shifted as well as skewed toward the red (best seen in the inset of panel A, where the peak region has been zoomed in). Fitting by the same template gave $\lambda_{max} = 504.6$ nm, but then the data points near peak still fell systematically above and to the right of the template and those farther in the red below and to the left of the template. Therefore, we applied an *ad hoc* parabolic fit to a narrow range around peak to get "local" estimates of the positions of the maxima (see panel A, inset). The domain was chosen to include all data points having normalized absorbance ≥ 0.9. Judged in this way, the peak shifted from 503.1 nm (28.5°C) to 504.2 nm (8.5°C).

When the data are plotted on logarithmic ordinates (panel B), a second effect becomes conspicuous: the relative sensitivity to very long wavelengths is higher at the higher temperature. In this plot, a wavenumber ($1/\lambda$) abscissa is used to enable comparison with the predictions of Stiles' (1948) model (see Methods). First, there is indeed an approximately linear decline of log sensitivity with decreasing photon energy ($\propto 1/\lambda$) in the far red. This is best seen in Fig. 3A, where the long-wavelength region from Fig. 2 is replotted on expanded scales. Second, the slopes of the straight lines fitted by weighted linear regression to the data (each data point was weighted by $1/\text{SEM}^2$) are on the order of magnitude predicted by theory (slope $hc/kT \ln 10$), albeit slightly shallower. The regression slopes 1.684×10^{-5} m (cold) and 1.570×10^{-5} m (warm) are *ca.* 76% of the predicted values, where Stiles (1948) found 79% for the human rod spectrum and Lamb (1984) 75% for single toad rods. Third, and most significantly, the *ratio* of the slopes is in excellent agreement with the theory's prediction that slopes should be proportional to $1/T$. The cold/warm slope ratio is $1.684/1.570 = 1.073$, to be compared with the inverse ratio of the experimental temperatures, 301.7 K / 281.7 K = 1.071.

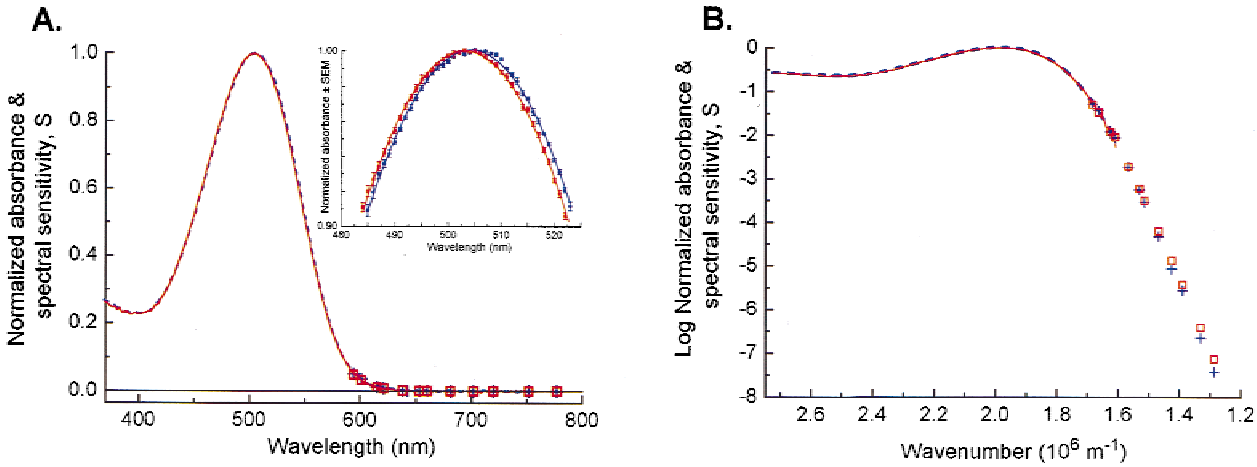

Fig. 2. (A) Normalized composite spectrum (absorbance and sensitivity) of *Bufo marinus* red rods at 8.5°C ("cold") and 28.5°C ("warm"). MSP data are shown by lines: blue dashed line (cold) and red continuous line (warm). ERG data are shown by symbols: blue plus signs (cold) and open red squares (warm). The inset shows the MSP data around peak (normalized absorbance ≥ 0.9) at higher resolution: filled blue circles (cold) and red squares (warm). The curves in the inset are best-fitting second-order polynomials. The error bars refer to the SEM of MSP data recorded from five different animals with 40 cells in each recording. (B) The same data as in the main panel of (A) plotted as log-normalized absorbance or log-normalized spectral sensitivity against wavenumber ($1/\lambda$).

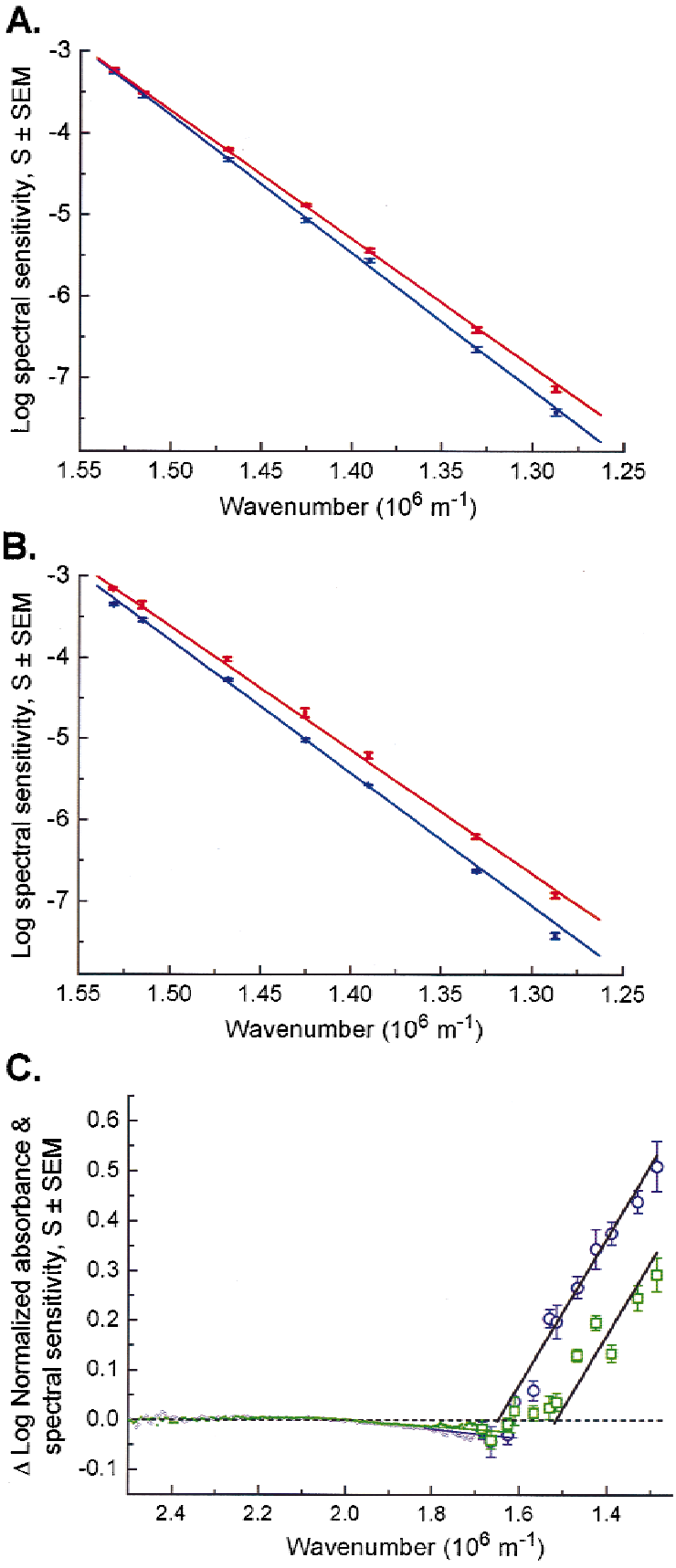

Fig. 3. The long-wavelength tail (653–777 nm) of *Bufo marinus* (A) and *Bufo bufo* (B) spectral sensitivity data at 8.5°C (blue) and 28.5°C (red), fitted with straight lines by weighted regression. The data points are means of recordings from eight (*Bufo marinus*) and four (*Bufo bufo*) retinas (data tabulated in Tables 1 and 2 in the Appendix). In the regression analysis, points were weighted by the factor $1/\mathrm{SEM}^2$ (the SEM values are shown as error bars). (C) Warm–cold difference spectra, showing the difference of spectral sensitivities at 28.5°C and 8.5°C ($\Delta\log S = \log S_W - \log S_C$). MSP data are shown by small, nearly confluent symbols (small open violet circles: *Bufo bufo*, small filled green squares: *Bufo marinus*). ERG data are shown by large symbols (open violet circles: *Bufo bufo*, open green squares: *Bufo marinus*). The error bars show SEMs. Straight black lines constrained to have the slope predicted by Stiles' model ($= -1.47\cdot10^{-6}$ m) have been positioned for best fits to those long-wavelength points for which $\Delta\log S \geq 0.1$. The dashed line shows the zero level corresponding to the normalization of cold and warm MSP spectra to the same peak value. The crossing points of the zero line and the "Stiles" fits to the long-wavelength points give simple graphical estimates of the activation energies, indicating in this case 43.4 kcal/mol for *Bufo marinus* and 47.1 kcal/mol for *Bufo bufo*.

Similar recordings were carried out in red rods of the closely related common toad, *Bufo bufo*. The values obtained were $\lambda_{max}(8.5°C) = 503.0$ nm, $\lambda_{max}(28.5°C) = 501.9$ nm; and final long-wavelength slopes 1.636×10^{-5} m (cold) and 1.522×10^{-5} m (warm). The long-wavelength slopes (displayed in Fig. 3B) were thus somewhat shallower than in *Bufo marinus*, but the ratio of slopes 1.075 remains close to the theoretically predicted value 1.071.

The activation energy

The temperature effect on the long-wavelength limb of spectra allows calculation of the photoactivation energy E_a. The procedure described in the Methods section applied to the data in Figs. 3A and 3B gives $E_a = 44.3 \pm 0.6$ kcal/mol for *Bufo marinus* and $E_a = 48.8 \pm 0.5$ kcal/mol for *Bufo bufo* red rods. The difference is statistically significant at the $P < 0.001$ level.

The anchoring of ERG data to MSP data here allowed us to rule out some potential error sources connected with ERG spectra near peak and at shorter wavelengths, for example, rhodopsin self-screening and intrusion of green-rod responses. Thus, it is gratifying that the present value for *Bufo bufo* is so close to the purely ERG-based estimate (49.2 kcal/mol) of Koskelainen et al. (2000). However, our rationale still builds on the (inaccurate) assumption that temperature affects spectra *only* in the far red. First, assessing the differences in relative sensitivities at long wavelengths always requires normalization of "cold" and "warm" spectra to coincide in some wavelength domain supposedly unaffected by temperature. Second, the logic requires that relative sensitivity changes result wholly from changes in the distribution of rhodopsin molecules on thermal energy levels; if any other effects of temperature extend into the domain used for estimating E_a, the results will be compromised.

To give a visual idea of the potential error due to the λ_{max} shift compared with the interspecies difference, we introduce another format of data presentation in Fig. 3C. Here, the warm–cold *differences* are plotted against $1/\lambda$ over both the MSP and ERG domains for both species. (See Methods for the anchoring of ERG difference data to the respective MSP difference spectra.) The provisional zero level (dashed horizontal line) plotted for visual guidance corresponds to our previous normalization of MSP spectra to have the same peak value. Upward deviations indicate relative increases in "warm" sensitivities, downward deviations the opposite. In the ideal "Stiles" case, difference spectra would follow this baseline exactly, until the relative increase in "warm" sensitivities starts to appear as a monotonical rise in the long-wavelength range. The solid straight black lines describing this rise in Fig. 3C have been constrained to have the slope predicted by theory, $hc(T_C - T_W)/kT_WT_C \ln 10$, which (for $T_C = 281.7$ K and $T_W = 301.7$ K) gives -1.47×10^{-6} m. They have been positioned for best fit to the data points that deviate by more than 0.1 log units from baseline, because in this range the predicted *slope* is the same in the Stiles (1948) and the Lewis (1955) formulations (see Discussion). The slope fits the *Bufo bufo* data (violet circles) well and is not inconsistent with the more scattered *Bufo marinus* data (green squares). On Stiles' theory, these lines intersect with the "true" baseline at λ_0, and thereby define $E_a = hc/\lambda_0$. The points of intersection with the provisional baseline in Fig. 3C suggest $E_a =$ 43.4 and 47.1 kcal/mol for *Bufo marinus* and *Bufo bufo*, respectively. However, the inadequacy of the model is evident as systematic deviations of the difference spectra from the zero line even elsewhere than in the long-wavelength domain, making it impossible in principle to define a "true" baseline.

The significance of such a systematic error can be evaluated only against the background of some supplementary "physical interpretation." Following Jurkowitz et al. (1959) (see Discussion), we suggest that the λ_{max} shift and other changes around the peak of the spectrum reflect changes in the spacing of electronic energy states of the molecule, bringing with it a change in the photoactivation energy itself with temperature. This possible change in E_a cannot be calculated simply from the inverse λ_{max} ratio (e.g. 503.1/504.2 in *Bufo marinus* when going from warm to cold), because as shown here and by Koskelainen et al. (2000), E_a is not necessarily proportional to $1/\lambda_{max}$. Instead, we calculate how much the E_a estimate is changed, if the spectra are shifted back into register with respect to λ_{max} (e.g. the "cold" spectrum is moved from 504.2 nm to 503.1 nm). Applying our standard procedure for E_a estimation to the *shifted* spectra gives a difference of *ca.* 0.5 kcal/mol compared with the original estimate. It should be noted that since the λ_{max} shifts in both species go in the same direction and are similar in size, the same will be true of the potentially resulting error in E_a.

Dependence of λ_{max} on temperature

To get a fuller picture of the temperature dependence of λ_{max}, we studied the *Bufo marinus* rhodopsin spectrum by MSP at two additional temperatures (0°C & 38°C) outside the original, strictly "physiological" range. The mean values ± SEM of λ_{max} at each of the four temperatures (determined as shown in Fig. 2A, inset) are plotted in Fig. 4 (circles with error bars). The temperature dependence might be quite satisfactorily described by a straight line with slope −0.06 nm/°C: if temperature in °C is denoted x and λ_{max} in nm denoted y, the linear regression equation is $y = -0.060x + 504.7$ ($r^2 = 0.993$). Since the data show a slight but systematic

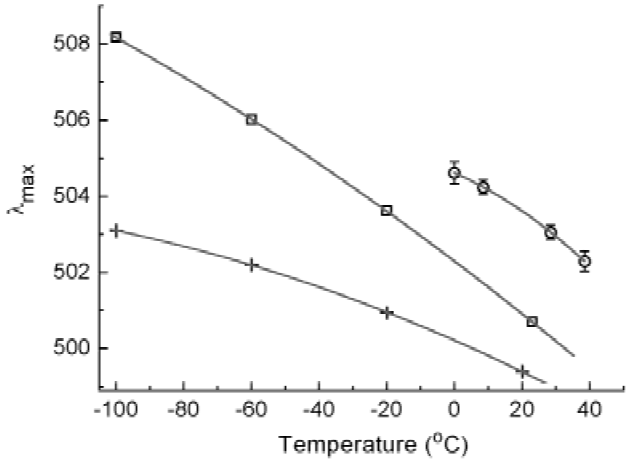

Fig. 4. The temperature dependence of λ_{max} (nm) in red rods of *Bufo marinus* (circles; error bars give SEMs) and in bullfrog (squares) and bovine (pluses) rhodopsin in solution. Toad λ_{max} was determined at each temperature by a parabolic fit to the peak of the spectrum as described in connection with Fig. 2A (inset). The bullfrog and bovine data were extracted from curves published by St. George (1952). The continuous lines are second-order polynomials ($y = A + Bx + Cx^2$) fitted to the data points (weighting the points by $1/\text{SEM}^2$ when fitting the toad data). The coefficients are $A = 500.2$ (bovine), 502.3 (bullfrog), 504.6 (toad); $B =$ −0.039 (bovine), −0.067 (bullfrog), −0.039 (toad); and $C = -0.00010$ (bovine), −0.000087 (bullfrog), −0.00056 (toad).

curvature, however, a second-order polynomial was fitted: $y = -0.00056x^2 - 0.039x + 504.6$ ($r^2 = 0.99999$). For comparison, the λ_{max} of bovine and bullfrog (*Rana catesbeiana*) rhodopsin measured in solution at several temperatures between −100 and +23°C have been extracted from the absorption curves published by St. George (1952) and plotted into the same graph. All the data sets have been fitted with second-order polynomials. The steepness of the temperature dependence in our toad rods is in good agreement with St.George's bullfrog rhodopsin data. A possible linear fit to the latter would give the same slope, −0.06 nm/°C ($y = -0.061x + 502.2$). Compared with the bovine pigment, however, the temperature effect on the two amphibian rhodopsins appears to be steeper. This shows that even within the red-rod family there are differences in the temperature dependence of λ_{max}. The parabolic fits in Fig. 4 do not intersect within the physiological temperature range (the extrapolated crossing point of the bovine and bullfrog curves would be at 77°C). Thus, the differences in body temperature between "cold-blooded" and "warm-blooded" animals can explain only an insignificant part of the differences in λ_{max} values reported in the literature.

Comparison between rhodopsin and the visual pigment of the green rods

Fig. 5 plots mean "warm" (38°C, red circles) and "cold" (0°C, solid blue curve) spectra recorded in green rods from three *Bufo marinus* retinas (42 cells at 38°C and 30 cells at 0°C). The green rods behave quite differently from the red rods. There is no perceptible shift in λ_{max}: when estimated by the same method that was used for the red rods, the two sets of data yield 432.5 nm (cold) and 432.7 nm (warm), respectively. In Fig. 6, the grand means of λ_{max} values obtained from measurements on green rods at 0°C and 38°C have been plotted together with the red-rod data and the parabolic curve fit to these, taken from Fig. 4. The two green-rod data points define the line $y = 432.54 + 0.003x$, where x is temperature (°C) and y is λ_{max} (nm). Thus, within an accuracy of 0.1 nm, the λ_{max} of green rods remained constant (432.6 nm) in the temperature range studied.

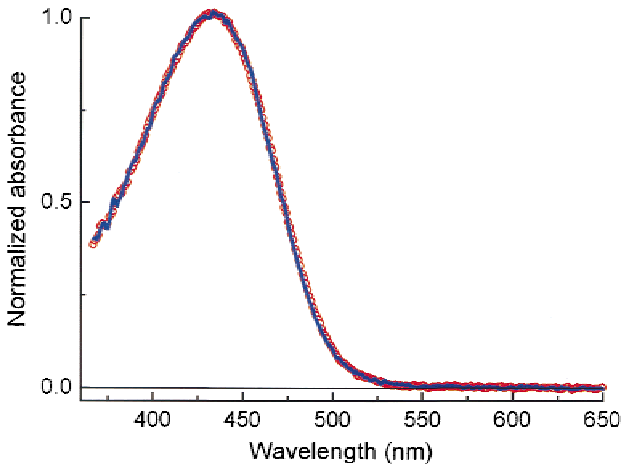

Fig. 5. Normalized absorbance spectra of green rods of *Bufo marinus* at 0°C (solid blue line) and 38°C (open red circles). The spectra are averages from 32 (at 0°C) and 42 (at 38°C) outer segments from three different animals.

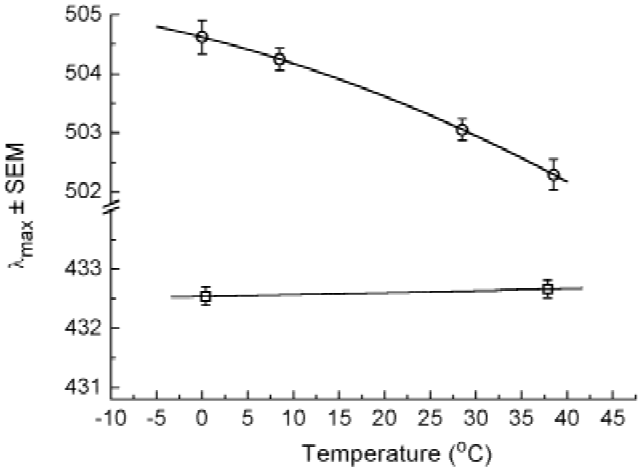

Fig. 6. The temperature dependence of λ_{max} (nm) in green rods (squares) of *Bufo marinus*, compared with the red-rod data from Fig. 4 (circles). λ_{max} was determined by a parabolic fit to the peak of the spectrum at each temperature (cf. Fig. 2A, inset). Error bars give SEMs. Green rods show no statistically significant temperature dependence of λ_{max}. Regression line for green rods: $y = 432.54 + 0.003x$.

In green rods, we were unable to measure a warming-induced increase in relative sensitivity at long wavelengths that would have allowed us to estimate E_a for the visual pigment. In the wavelength range where absorbance was sufficient to be reliably measured by MSP, up to ca. 530 nm, there was no indication of a warm–cold difference in relative sensitivities. Our ERG technique, on the other hand, did not allow us to record uncontaminated green-rod responses. Thus, we can only give a lower limit (530 nm) for the possible emergence of a temperature effect on long-wavelength sensitivity. This would suggest $E_a \leq 54$ kcal/mol. Proper estimation of the activation energy of the green-rod pigment will have to be based on data from single-cell electrophysiology, for example, suction-pipette recording.

Discussion

Lack of evidence of A2 chromophore

Instead of the common A1 chromophore (11-cis retinal), some fish, amphibians, and reptiles use the A2 chromophore (3-dehydroretinal) or a mixture of both A1 and A2 chromophores (Dartnall & Lythgoe, 1965). The A1 → A2 chromophore substitution broadens the absorbance spectra (Bridges, 1965), shifts its λ_{max} towards longer wavelengths (Dartnall & Lythgoe, 1965), and seems to decrease the energy needed for photoactivation of the pigment (E_a) (Koskelainen et al., 2000). Previous authors have found no evidence for the presence of A2 chromophore in the model species of this work *Bufo bufo* and *Bufo marinus* (Partridge et al., 1992; Govardovskii et al., 2000). The possibility of the presence of A2 was also checked by fitting the Govardovskii template to the warm (28.5°C) spectra. Both *Bufo marinus* and *Bufo bufo* spectra were best fitted by the pure A1 template. The Govardovskii template containing even a small fraction of A2 pigment (*ca.* 1%) deviates clearly from the measured spectra. Thus, all the results of this paper are believed to reflect temperature properties of pure A1 pigments.

The temperature dependence of λ_{max}

The absorbance peak of rhodopsin shifted toward shorter wavelengths with rising temperature as summarized in Fig. 4. In a linear approximation, the change amounted to −0.6 nm per 10°C temperature rise. Toad rhodopsin *in situ* in functioning rods thus shows very similar behaviour to bovine and bullfrog rhodopsin in solution (Fig. 4; cf. St. George, 1952). Interestingly, the A1 chromophore alone (11-cis retinal not coupled to opsin), as well as several other carotenoids, shows quite similar red shifts with cooling (0.6–1.0 nm per 10°C), even though the absorbance maximum of the 11-cis A1 chromophore at room temperature lies at more than 130 nm shorter wavelength than that of the intact pigment (Jurkowitz et al., 1959).

The absorbance spectrum of a visual pigment is the probability distribution for electronic excitations from the ground state to the first excited state as a function of photon energy. The width and the continuity of the distribution is due to the large number of thermal energy levels associated with each electronic state, offering a rich complement of possible transitions with different energies. The wavelength of peak absorption, λ_{max}, corresponds to the energy (hc/λ_{max}) at which the summed probability of possible transitions is greatest. By contrast, the spectra of the chromophore alone and related molecules, studied by Jurkowitz et al. (1959) from room temperature down to −195°C, do show fine structure corresponding to vibrational levels at least in the cold. For example, *all-trans* β-carotene has five sharp peaks in the "cold" spectrum and at least three of these are discernible even at room temperature. From this, the authors could show that all the peaks shifted about equally with temperature, consistent with a common lowering of all the energy levels of the first excited state relative to the ground state upon cooling. It is natural to think that the spectrum of rhodopsin shifts as a whole in similar manner. One particular implication is that the lowest-energy transition, corresponding to our "activation energy" E_a, must then also be temperature dependent (see below).

In rhodopsins as well as the L and M2 cone visual pigments (to use the terminology of Okano et al., 1992), the interaction between the chromophore and the opsin serves to tune absorbance to significantly longer wavelengths than that of the protonated chromophore Schiff base alone (λ_{max} = 440 nm). At least for the rhodopsins, it appears to be a universal rule that cooling shifts λ_{max} toward longer wavelengths (although there may be some variation in the exact form of the shift, see Fig. 4). By contrast, the green-rod pigment, which is tuned to (slightly) *shorter* wavelengths than the protonated chromophore Schiff base, showed no measurable temperature dependence of λ_{max}. Amphibian green-rod pigments represent the M1 family of "blue" cone pigments, where λ_{max} of other members range from 430 nm to 470 nm (Hisatomi et al., 1999; Ma et al., 2001). Two members of the family of "UV-violet" or S cone pigments (peaking at *ca.* 350−450 nm) have been studied at low temperature by Vought et al. (1999). Of these, the "violet" cone pigment of *Xenopus* (λ_{max} = 426 nm) showed no spectral shift with cooling, consistent with our present result on green rods. The strongly short-wave-tuned mouse UV pigment (λ_{max} = 357 nm at room temperature) was red shifted by 4 nm upon cooling to 70 K, that is, changed in the same direction but much less than rhodopsin or isolated chromophore in solution. Vought et al. (1999) proposed that the mouse UV chromophore is initially unprotonated, in contrast to the situation in most visual pigments. The available evidence suggests that there is considerable variety in the mechanisms underlying spectral tuning in visual pigments.

Species differences in λ_{max} persist over the physiological temperature range

The λ_{max} value for *Bufo marinus* interpolated to room temperature from our present data (Fig. 4) is 503.6 nm, in fair agreement with earlier MSP work giving 503.2–503.4 nm (Fyhrquist et al., 1998*b*; Govardovskii et al., 2000). Differences in λ_{max} of *ca.* 2 nm compared with *Rana catesbeiana* rhodopsin (501.5 nm at room temperature: Reuter et al., 1971) and > 4 nm compared with bovine rhodopsin (cf. Partridge & de Grip, 1991) persist essentially unchanged over the whole temperature range (0°C–38°C). For example, the parabolas describing the bovine and the bullfrog pigments in Fig. 4 would intersect only at *ca.* 77°C, far outside the physiological range.

The visual pigment template

Govardovskii et al. (2000) showed that the original idea of Dartnall (1953) that all visual pigments can be described by a common template with λ_{max} as sole variable is still basically valid (although the templates are different for the two chromophores A1 and A2). Their templates describe all recorded spectra (with λ_{max} ranging from 357 nm to 620 nm) with an accuracy within measurement error. They do not, however, take temperature effects into account. It might be rather a simple mathematical exercise to incorporate a reasonable description of the λ_{max} shift and change in long-wavelength slope with temperature. The temperature effects, however, are too small to seriously modulate the spectral sensitivity of the animal in an ecological sense, so there is hardly a pressing demand for such formulations.

Reliability of the E_a estimate and the difference between Bufo marinus and Bufo bufo

One important objective of the present work has been to evaluate sources of error in our procedures for estimating the activation energy E_a. Two problems connected with the ERG signal itself (rhodopsin self-screening and intrusion of response components from other photoreceptors) are avoided by our present strategy of anchoring long-wavelength ERG data to MSP spectra. When comparing these values with those obtained from analysis of ERG data alone (44.3 *vs.* 43–44 kcal/mol in *Bufo marinus*, 48.8 *vs.* 49.2 kcal/mol in *Bufo bufo*), we find that the effect of these factors is small. In fact, a small amount of self-screening is present in the MSP spectra. This effect was not corrected, because its effect on E_a estimates was shown to be negligible (< 0.1 kcal/mol).

A more troublesome source of error is the imperfection of the underlying theory, which fails to accommodate the temperature dependence of spectra around peak. As argued above, the shift in λ_{max} is likely to indicate a small change in E_a itself. On this interpretation, we applied the correction of shifting the "cold" and the "warm" spectrum into register on the wavenumber scale and calculated E_a from the relative long-wave sensitivities of the shifted spectra. This correction changed E_a by only *ca.* 0.5 kcal/mol. This is little compared with the species difference. Moreover, since the λ_{max} shift is similar in both species, a possible systematic error due to this should also go in the same direction, preserving the relation between species.

However, in the absence of strict quantum physical modelling of the rhodopsin molecule (which is not yet feasible at the required resolution), the unquestionable experimental differences in temperature effect on long-wavelength sensitivity (Fig. 3) are of

course in principle open to different interpretations, depending on the model used. For example, Lewis' (1955) formulation (see Methods) offers the option of partitioning differences between two parameters, E_a and m, where the latter corresponds to the effective degrees of freedom in the vibrational energy modes of the molecule (cf. Hinshelwood, 1940). Lewis' formula with our present E_a estimates and $m = 3$ provides excellent fits to the long-wavelength limbs of both "warm" and "cold" spectra of both species (it will be remembered that Stiles' formula predicts too steep absolute slopes). Acceptable fits can also be obtained with $m = 4$, 5, or 6 and slightly higher E_a, but unless it is arbitrarily assumed that similar spectra arise from quite different combinations of m and E_a, the choice will affect the E_a estimates for the two species similarly. The *difference* in activation energies between *Bufo marinus* and *Bufo bufo* rhodopsins thus appears as robust, although, for example, fitting Lewis' model with m values > 3 would raise the E_a estimates for both.

Spectra, activation energy, and thermal noise

Developing the implications of Stiles' (1948) theory, Barlow (1957) proposed the idea of a necessary physical connection between the position of the absorbance spectrum of a visual pigment and its propensity to undergo spontaneous thermal isomerization. He reasoned that tuning to long-wavelength light (low-energy photons) is equivalent to having a low energy barrier for activation, hence being comparatively easily activated by thermal energy alone. The implications are of considerable biological significance, as two important functional variables of visual pigments, spectral photon catch and the production of false light-like signals (background noise), would then be interconnected. An increase in red sensitivity would always bring a cost in increased noisiness and natural selection in a light environment rich in long wavelengths would have to balance between increased quantum catch and increased noise (cf. Donner et al., 1990; Firsov & Govardovskii, 1990). In this and previous work (Koskelainen et al., 2000), our goal has been to test some aspects of Barlow's (1957) idea by measuring the quantity assumed to connect spectral and thermal properties, the activation energy E_a. In view of later studies on the activation energy for *thermal* events (see below), it must be emphasized that E_a as we define it is the minimum energy for *photo*activation of the visual-pigment molecule starting from the zero-vibrational level of the ground state. To date, measuring the temperature effect on relative spectral sensitivities at long wavelengths appears to provide the only means for obtaining sufficiently accurate estimates of this quantity.

The presently available data on E_a, λ_{max}, and thermal isomerizations force the *negative* conclusion that, contrary to the attractive theory of Barlow (1957), there is no "strong", physically necessary connection between any two of these properties. (1) Similar λ_{max} may be associated with very different rates of spontaneous thermal isomerizations [rhodopsins of *Bufo marinus vs. Rana catesbeiana*: Baylor et al. (1980) and Donner et al., (1990)]; (2) Similar λ_{max} and thermal isomerization rate may be connected with significantly different activation energies (rhodopsins of *Bufo marinus vs. Bufo bufo*: present work compared with Fyhrquist et al., (1998*b*) and Firsov et al. (2002)); (3) Very different λ_{max} may be connected with indistinguishable activation energies [rhodopsin *vs.* L-cone pigment of *Rana temporaria*: Koskelainen et al. (2000)].

The decoupling of photoactivation and thermal activation parameters is in line with the present consensus that the two types of activation follow different molecular routes. This conclusion is mainly based on the very much lower Arrhenius activation energies for thermal activation (20–25 kcal/mol), as derived from the temperature dependence of electrical photon-like noise in rods and cones (Baylor et al., 1980; Matthews, 1984; Sampath & Baylor, 2002).

On the other hand, one should not jump to a hasty conclusion that no *correlations* of the kind predicted by Barlow (1957) exist. The data only refute the idea of a strong physical coupling of the three properties. Indeed, in the case of a chromophore switch from retinal A1 to A2 in the same opsin, all three move in the predicted direction: λ_{max} is red shifted, E_a decreases, and thermal noise goes up (Donner et al., 1990; Koskelainen et al., 2000). When the rate of thermal photon-like "dark" events is plotted against λ_{max} for all species of "red" rods that have been investigated in this respect, a significant positive correlation emerges (Firsov & Govardovskii, 1990; Fyhrquist, 1999). To explain these correlations, it is still necessary to consider the relation between photoactivation and apparent thermal activation energies of visual pigments.

In green rods, we were unable to measure any relative increase in long-wavelength sensitivity with warming. This suggests that E_a is too low for temperature effects to appear in the range we can record reliably by MSP (up to *ca.* 530 nm, suggesting $E_a < 54$ kcal/mol). Our ERG mass receptor recording is useless for extending the measurable spectrum of the green rods, as the long-wavelength end is submerged under a dominant red-rod signal. Determination of E_a for the green-rod pigment will have to await single-cell electrophysiological recording.

Acknowledgments

We are grateful to Dr. Victor Govardovskii for constructing the microspectrophotometer used in this work and for critically reading the manuscript. We also thank Mr. Sami Minkkinen for skilful technical assistance. This work was supported by the Academy of Finland (grants 49947, 51681, and 36154) and by the Finnish Graduate School of Molecular Nanotechnology.

References

Alpern, M., Fulton, A.B. & Baker, B.N. (1987). "Self-screening" of rhodopsin in rod outer segments. *Vision Research* **27**, 1459–1470.

Barlow, H.B. (1957). Purkinje shift and retinal noise. *Nature* **179**, 255–256.

Baylor, D.A., Hodgkin, A.L. & Lamb, T.D. (1974). The electrical response of turtle cones to flashes and steps of light. *Journal of Physiology* **242**, 685–727.

Baylor, D.A., Lamb, T.D. & Yau, K.-W. (1979). The membrane current of single rod outer segments. *Journal of Physiology* **288**, 589–611.

Baylor, D.A., Matthews, G. & Yau, K.-W. (1980). Two components of electrical dark noise in toad retinal rod outer segments. *Journal of Physiology* **309**, 591–621.

Bolnick, D.A., Walther, A.E. & Sillman, A.J. (1979). Barium suppresses slow PIII in perfused bullfrog retina. *Vision Research* **19**, 117–119.

Bridges, C.D.B. (1965). Absorption properties, interconversions, and environmental adaptation of pigments from fish photoreceptors. *Cold Spring Harbor Symposia on Quantitative Biology* **30**, 317–334.

Dartnall, H.J.A. (1953). The interpretation of spectral sensitivity curves. *British Medical Bulletin* **9**, 24–30.

Dartnall, H.J.A. & Goodeve, C.F. (1937). Scotopic luminosity curve and the absorption spectrum of visual purple. *Nature* **139**, 409–411.

Dartnall, H.J.A. & Lythgoe, J.N. (1965). The spectral clustering of visual pigments. *Vision Research* **5**, 81–100.

de Vries, H. (1948). Der Einfluss der Temperatur des Auges auf die spektrale Empfindlichkeitskurve. *Experientia* **4**, 357–358.

Donner, K.O. & Reuter, T. (1976). Visual pigments and photoreceptor function. In *Frog Neurobiology*, ed. Llinás, R. & Precht, W., pp. 251–277. Berlin-Heidelberg-New York: Springer.

Donner, K. & Hemilä, S. (1985). Rhodopsin phosphorylation inhibited by adenosine in frog rods: Lack of effects on excitation. *Comparative Biochemistry and Physiology* **81A**, 431–439.

Donner, K., Hemilä, S. & Koskelainen, A. (1988). Temperature-dependence of rod photoresponses from the aspartate-treated retina of the frog (*Rana temporaria*). *Acta Physiologica Scandinavica* **134**, 535–541.

Donner, K., Firsov, M.L. & Govardovskii, V.I. (1990). The frequency of isomerization-like "dark" events in rhodopsin and porphyropsin rods of the bull-frog retina. *Journal of Physiology* **428**, 673–692.

Firsov, M.L. & Govardovskii, V. .I. (1990). Dark noise of visual pigments with different absorption maxima. *Sensornye Sistemy* **4**, 25–34 (in Russian).

Firsov, M.L., Donner, K. & Govardovskii, V.I. (2002). pH and rate of 'dark' events in toad retinal rods: Test of a hypothesis on the molecular origin of photoreceptor noise. *Journal of Physiology* **539**, 837–846.

Fyhrquist, N. (1999). Spectral and thermal properties of amphibian visual pigments related to molecular structure. *Dissertationes Biocentri Viikki Universitatis Helsingiensis* **18/99**.

Fyhrquist, N., Donner, K., Hargrave, P. A., McDowell, J.H., Popp, M.P. & Smith, W.C. (1998*a*). Rhodopsins from three frog and toad species: Sequences and functional comparisons. *Experimental Eye Research* **66**, 295–305.

Fyhrquist, N., Govardovskii, V., Leibrock, C. & Reuter, T. (1998*b*). Rod pigment and rod noise in the European toad *Bufo bufo*. *Vision Research* **38**, 483–486.

Good, N.E., Winget, G.D., Winter, W., Connolly, T.N., Izawa, S. & Singh, R.M. (1966). Hydrogen ion buffers for biological research. *Biochemistry* **5**, 467–477.

Govardovskii, V.I., & Zueva, L.V. (2000). Fast microspectrophotometer for studying the photolysis of visual pigments *in situ*. *Sensornye Sistemy* **14**, 288–296 (in Russian).

Govardovskii, V.I., Fyhrquist, N., Reuter, T., Kuzmin, D.G., & Donner, K. (2000). In search of the visual pigment template. *Visual Neuroscience* **17**, 509–528.

Harned, H.S. & Bonner, F.T. (1945). The first ionization of carbonic acid in aqueous solutions of sodium chloride. *Journal of the American Chemical Society* **67**, 1026–1031.

Hinshelwood, C.N. (1940). *The Kinetics of Chemical Change*. Oxford: Clarendon Press.

Hisatomi, O., Takahashi, Y., Taniguchi, Y., Tsukahara, Y. & Tokunaga, F. (1999). Primary structure of a visual pigment in bullfrog green rods. *FEBS Letters* **447**, 44–48.

Jurkowitz, L., Loeb, J.N., Brown, P.K. & Wald, G. (1959). Photochemical and stereochemical properties of carotenoids at low temperatures. *Nature* **184**, 614–624.

Koskelainen, A., Hemilä, S. & Donner, K. (1994). Spectral sensitivities of short- and long-wavelength sensitive cone mechanisms in the frog retina. *Acta Physiologica Scandinavica* **152**, 115–124.

Koskelainen, A., Ala-Laurila, P., Fyhrquist, N. & Donner, K. (2000). Measurement of thermal contribution to photoreceptor sensitivity. *Nature* **403**, 220–223.

Krause, W. (1892). Die Retina. III. Die Retina der Amphibien. *Internationale Monatsschrift für Anatomie und Physiologie* **9**, 151–236.

Lamb, T.D. (1984), Effects of temperature changes on toad rod photocurrents. *Journal of Physiology* **346**, 557–578.

Lamb, T.D. (1995). Photoreceptor spectral sensitivities: Common shape in the long-wavelength region. *Vision Research* **35**, 3083–3091.

Lewis, P.R. (1955). A theoretical interpretation of spectral sensitivity curves at long wavelengths. *Journal of Physiology* **130**, 45–52.

Liebman, P.A. & Entine, G. (1968). Visual pigments of frog and tadpole (*Rana pipiens*). *Vision Research* **8**, 761–775.

Ma, J.-X., Znoiko, S., Othersen, K.L., Ryan, J.C., Das, J., Isayama, T., Kono, M., Oprian, D.D., Corson, D.W., Cornwall, M.C., Cameron, D.A., Hárosi, F.I., Makino, C.L. & Crouch, R.K. (2001). A visual pigment expressed in both rod and cone photoreceptors. *Neuron* **32**, 451–461.

MacNichol, E.F., Jr. (1986). A unifying presentation of photopigment spectra. *Vision Research* **26**, 1543–1556.

Matthews, G. (1984). Dark noise in the outer segment membrane current of green rod photoreceptors from toad retina. *Journal of Physiology* **349**, 607–618.

Newman, E.A. (1989). Potassium conductance block by barium in amphibian Müller cells. *Brain Research* **498**, 308–314.

Okano, T., Kojima, D., Fukada, Y., Shichida, Y. & Yoshizawa, T. (1992). Primary structure of chicken cone visual pigments: Vertebrate rhodopsins have evolved out of cone visual pigments. *Proceedings of the National Academy of Sciences of the U.S.A.* **89**, 5932–5936.

Partridge, J.C. & de Grip, W.J. (1991). A new template for rhodopsin (vitamin A1 based) visual pigments. *Vision Research* **31**, 619–630.

Partridge, J.C., Speare, P., Shand, J., Muntz, W.R.A. & Williams, D.M. (1992). Microspectrophotometric determinations of rod visual pigments in some adult and larval Australian amphibians. *Visual Neuroscience* **9**, 137–142.

Reuter, T.E., White, R.H. & Wald, G. (1971). Rhodopsin and porphyropsin fields in the adult bullfrog retina. *Journal of General Physiology* **58**, 351–371.

Sampath, A.P. & Baylor, D.A. (2002). Molecular mechanism of spontaneous pigment activation in retinal cones. *Biophysical Journal* **83**, 184–193.

Srebro, R. (1966). A thermal component of excitation in the lateral eye of *Limulus*. *Journal of Physiology* **187**, 417–425.

St. George, R.C.C. (1952). The interplay of light and heat in bleaching rhodopsin. *Journal of General Physiology* **35**, 495–517.

Stiles, W.S. (1948). The physical interpretation of the spectral sensitivity curve of the eye. In *Transactions of the Optical Convention of the Worshipful Company of Spectacle Makers*, pp. 97–107. London: Spectacle Makers' Co.

Vega, C.A. & Bates, R.G. (1976). Buffers for the physiological pH range: Thermodynamic constants for four substituted aminoethanesulfonic acids from 5 to 50°C. *Analytical Chemistry* **48**, 1293–1296.

Vought, B.W., Dukkipatti, A., Max, M., Knox, B.E. & Birge, R.R. (1999). Photochemistry of the primary event in short-wavelength visual opsins at low temperature. *Biochemistry* **38**, 11287–11297.

Yoshizawa, T. (1972). The behaviour of visual pigments at low temperatures. In *Handbook of Sensory Physiology, VII/1. Photochemistry of Vision*, ed. Dartnall, H.J.A., pp. 147–179. Berlin-Heidelberg-New York: Springer.

Appendix

Table 1. *Spectral sensitivity of Bufo marinus red rods at 8.5°C ("cold", C) and 28.5°C ("warm", W)*[a]

λ (nm)	Wavenumber (10^6 m^{-1})	log S_W	log S_C	s.d.$_W$	s.d.$_C$	n_W	n_C
653	1.531	−3.230	−3.250	0.057	0.060	5	5
660	1.515	−3.508	−3.538	0.035	0.081	7	7
681	1.468	−4.200	−4.325	0.042	0.056	7	8
701.6	1.425	−4.879	−5.069	0.037	0.067	7	8
719.5	1.390	−5.433	−5.562	0.059	0.071	7	8
751.6	1.330	−6.412	−6.652	0.095	0.094	7	8
777	1.287	−7.134	−7.421	0.081	0.115	5	8

[a]λ = wavelength; s.d. = standard deviation; n = the number of points comprising the average. Results are plotted in Fig. 3A.

Table 2. *Spectral sensitivity of Bufo bufo red rods at 8.5°C ("cold", C) and 28.5°C ("warm", W)*[a]

λ (nm)	Wavenumber (10^6 m^{-1})	log S_W	log S_C	s.d.$_W$	s.d.$_C$	n_W	n_C
653	1.531	−3.156	−3.348	0.025	0.034	3	4
660	1.515	−3.353	−3.538	0.080	0.038	3	4
681	1.468	−4.016	−4.271	0.047	0.030	3	4
701.6	1.425	−4.679	−5.011	0.096	0.039	3	4
719.5	1.390	−5.203	−5.566	0.061	0.009	3	4
751.6	1.330	−6.199	−6.626	0.050	0.030	3	4
777	1.287	−6.924	−7.421	0.048	0.065	2	3

[a]λ = wavelength; s.d. = standard deviation; n = the number of points comprising the average. Results are plotted in Fig. 3B.